Research Article Vol. 30, No. 6 / 14 Mar 2022 / Optics Express 9983
Optics EXPRESS

Side-lobe reduction by cascading Bragg grating filters on a Si-photonic chip

SUSHANT KUMAR,[1,2,4] NAIF ALSHAMRANI,[1,3,4,*] ANDREW GRIECO,[1] AND YESHAIAHU FAINMAN[1]

[1]*Department of Electrical and Computer Engineering, University of California, San Diego, 9500 Gilman Dr., La Jolla, California 92093, USA*
[2]*Currently with The Institute of Optics, University of Rochester, 480 Intercampus Dr., Rochester, New York 14627, USA*
[3]*King Abdulaziz City for Science and Technology (KACST), P.O. Box 6086, Riyadh 11442, Saudi Arabia*
[4]*Co-first authors with equal contribution*
[*]*naalsham@eng.ucsd.edu*

Abstract: Bragg-grating based cavities and coupler designs present opportunities for flexible allocation of bandwidth and spectrum in silicon photonic devices. Integrated silicon photonic devices are moving toward mainstream, mass adoption, leading to the need for compact Bragg grating based designs. In this work we present a design and experimental validation of a cascaded contra-directional Bragg-grating coupler with a measured main lobe to side-lobe contrast of 12.93 dB. This level of performance is achieved in a more compact size as compared to conventional apodized gratings, and a similar design philosophy can be used to improve side-lobe reduction in grating-based mirror design for on-chip lasers and other cavity-based designs as well.

1. Introduction

As silicon photonic devices continue their drive into the mainstream applications, the need for high contrast, compact Bragg-grating devices is ever-present. These devices offer great potential for large scale photonic integration due to their small foot-print and low fabrication costs in addition to flat-top response, low insertion loss and wavelength tunability. Over the years there have been tremendous efforts to design and optimize such optical filters [1–10]. One example is the all-pass filter decomposition approach by Madsen which has a large footprint and high fabrication complexity. In addition, many designs based on apodised Bragg gratings show excellent main-lobe to side-lobe contrast [1,2,11], but such devices achieve the high contrast at the expense of broadening the main lobe and increasing the device length. As shown by the prior work done in [1] and [2],the apodised designs are not only long (approaching 1 mm in length) but also compromise the bandwidth and spectrum profile.

This behavior is not surprising or novel. It was discussed extensively in Kogelnik's original work [12], where it was shown that for a same device length the side-lobe reduction is achieved at the expense of higher peak coupling coefficient of the grating and wider main lobe. It should be noted that the peak coupling in a grating can't be increased arbitrarily, since the theoretical model relies on Perturbation theory to apply Coupled-mode equations. In [12] it is also shown that such devices are very sensitive to fabrication tolerances. In [12] when comparing Blackman and Kaiser apodization window functions, it is demonstrated how the two differ by less than 1% but their side lobes differ by 16dB. In addition, to achieve lower side lobes the apodization needs to be extremely smooth which results in bigger device footprint, and which can be difficult to fabricate in commercial foundries. Additional relevant numerical calculations and simulations can be found in [13,14].

#446588 https://doi.org/10.1364/OE.446588
Journal © 2022 Received 21 Oct 2021; revised 28 Feb 2022; accepted 28 Feb 2022; published 10 Mar 2022

Optics EXPRESS

In this manuscript, we propose and experimentally demonstrate a novel method for reduction of side lobes via cascaded contra-directional couplers (CDC_S) utilizing Bragg gratings. As opposed to previous demonstrations, where such reduction is achieved via apodization of the Bragg grating, we design non-similar gratings in each of the contra-directional couplers. Each coupler is designed so that the null of the main lobe of the first grating coupler, overlaps with the peak of the side lobe of the second grating coupler. In our experiments, the gratings were tuned thermo-optically to match their central frequencies.

2. Theory and design

The effect of the periodic perturbation on a waveguide can be described by coupled-mode theory, which is noted in [15]. According to the coupled-mode theory the main effect of a periodic perturbation is to transfer energy from one mode to another. Such a transfer occurs when a difference between the mode wavenumbers is equal to that of the grating wavenumber, which is also known as the phase matching condition. Moreover, the strength of the coupling is determined by a quantity known as the coupling coefficient, which depends on the overlap between the interacting modes and the perturbation. For example, the periodic perturbation in direction of propagation x, the perturbation in permittivity can be decomposed into a Fourier series as follows [14–16]:

$$\Delta\varepsilon(x,y,z) = \sum_l \Delta\varepsilon_l(y,z)\exp\left(-il\frac{2\pi x}{\Lambda}\right) \tag{1}$$

where Λ is the period of the perturbation, ε refers to the permittivity, l indicates the order of the Fourier series term in consideration, x, y and z are the cartesian coordinates. This can then be used in Eq. (6) to determine the coupling strength between the modes of interest. In this work, only the first order perturbation term was taken into consideration and the periodicity of perturbation for each set of contra-directional couplers was set using Eq. (7). The propagation constant (β_i) and the electric field profiles required for each mode in consideration can be calculated using any electromagnetic mode solver (i.e., LUMERICAL MODE). Once those above quantities are obtained, they can be substituted in Eq. (6) and Eq. (7) to obtain the coupling coefficient k_{lnm} and the periodicity of the perturbation Λ. Since wider waveguides have more confined modes, the overlap between modes is reduced. Finally, the differential equations govern such interactions are shown below [1,15,16]:

$$\frac{dA_1}{dx} = -jk_{11}A_2e^{j2\Delta\beta_1 x} - jk_{12}B_2e^{j(\Delta\beta_1+\Delta\beta_2)x} \tag{2}$$

$$\frac{dB_1}{dx} = -jk_{12}A_2e^{j(\Delta\beta_1+\Delta\beta_2)x} - jk_{22}B_2e^{j2\Delta\beta_2 x} \tag{3}$$

$$\frac{dA_2}{dx} = jk_{11}^*A_1e^{-j2\Delta\beta_1 x} + jk_{12}^*B_1e^{-j(\Delta\beta_1+\Delta\beta_2)x} \tag{4}$$

$$\frac{dB_2}{dx} = jk_{12}^*A_1e^{-j(\Delta\beta_1+\Delta\beta_2)x} + jk_{22}^*B_1e^{-j2\Delta\beta_2 x} \tag{5}$$

Where k_{11}, k_{22}, k_{12} are the coupling coefficients, * symbolizes a complex conjugate, A_1 & B_1 are forward propagating modes in each waveguide pair, while A_2 & B_2 are backward propagating modes. For CDC_1, A_m represent the modes in Wg_1 while B_m represent modes in WG_2. Similarly, for CDC_2, A_m represent the modes in Wg_2 while B_m represent modes in WG_3. The methodology for solving above sets of coupled mode equations can be found in [1,15,16]. The above equations can be solved numerically, and the coupling coefficients can be varied to obtain the desired spectrum for each CDC. As mentioned before, the coupling coefficient can be tuned via multiple parameters like the gap between waveguides, the width of waveguide pairs, amount of perturbation. Then each individual CDC can be designed and simulated via FDTD or similar method to verify

Optics EXPRESS

the functionality of the device and make any final adjustments before fabrication. In this case, only the waveguide width (WG_1 & WG_3) was altered and all other parameters except periodicity were kept identical for each CDC to minimize the effects of any fabrication variations/errors.

In general, two-phase mismatched modes don't undergo significant coupling. To transfer power between such modes, a Bragg grating based coupler relies on periodic perturbations. The perturbations determine the strength of coupling between the modes while the periodicity is chosen to compensate for the phase mismatch between the modes under consideration. The response of such devices usually consists of a strong main lobe and side peaks at frequencies that are unwanted in the design. Coupling strength is a primary contributor to the strength and the width of the main lobe. But, at the same time the strong coupling also contributes to the strength of the unwanted side lobes. To overcome this, devices with weaker coupling strength can be engineered [12,14]. Another solution is to apodize the coupling coefficient over the device length [1,2,11,12]. In such cases, the device length is increased significantly while also making the devices more susceptible to fabrication errors.

The device in consideration consists of three dissimilar waveguides on 220nm Silicon on Insulator (SOI) platform. They are enumerated as Waveguides 1, 2 and 3 and will be referred to as WG_1, WG_2, and WG_3 from now on (see lay out shown in Fig. 1). The dissimilar waveguide widths ensure phase mismatch between TE_0 modes of the closely spaced waveguides and hence there is little to no co-directional coupling as the light propagates in any of the waveguides. The Bragg structures are obtained by creating perturbations in WG_1 and WG_3 similar to these in [17]. The coupling between relevant modes can be calculated by [14]:

$$k_{\ln m} = \frac{\omega \iint \Delta\varepsilon_l(y,z)(E_m^* \cdot E_n^*)dydz}{2 \iint \varepsilon(E_m^* \cdot H_n^*)dydz} \tag{6}$$

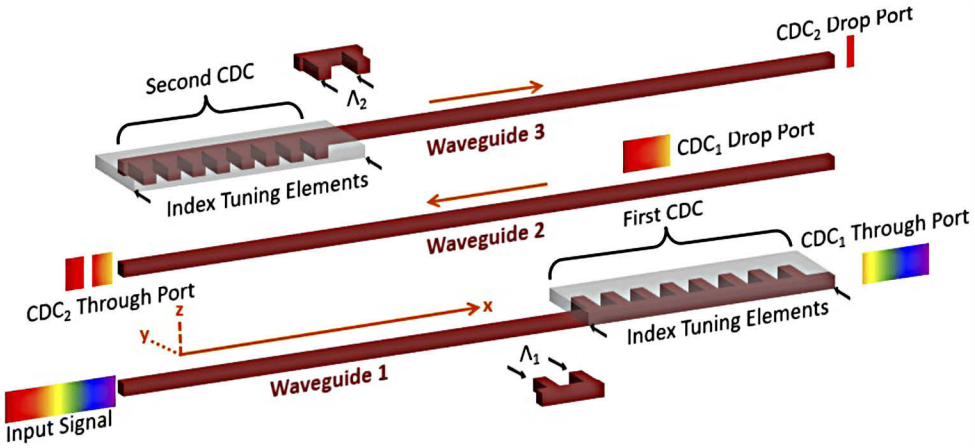

Fig. 1. Conceptual schematic diagram of a cascaded contra-directional couplers (CDCs) device created through coupled Bragg gratings. In this design CDC_1 redirects a segment of the input signal from waveguide 1 (WG_1) into waveguide 2 (WG_2) while the remaining spectra passes through (CDC_1 through port). Moreover, CDC_2 redirects the incoming signal from waveguide 2 into waveguide 3 (WG_3) such that the null of the main lobe of the first grating coupler, overlaps with the peak of the side lobe of the second grating coupler.

Here k_{lnm} describes the strength of coupling between the n^{th} mode and m^{th} mode due to the l^{th} order perturbation term, E_m refers to the electric field associted with the m^{th} mode, E_n refers to the electric field associted with the n^{th} mode, H_n refers to the magnetic field associted with the mode E_n, * symbolizes a complex conjugate, ω refers to the angular frequency of the optical field,

Optics EXPRESS

ε refers to the permittivity, l indicates the order of the Fourier series term, x is the direction of propagation while y and z are coordinates in the transverse plane. It should be noted that in such devices, every mode strictly speaking interacts with every other mode. But over long interatction lengths phase mismatches lead to negligible average coupling between the modes. This leads to the need for periodicity in perturbation.

The effective indices were calculated for unperturbed waveguides using commercial simulation software LUMERICAL MODE. Then the periodicity of perturbations for each waveguide pair were calculated to compensate for the difference in propagation constants using [14,15]:

$$\beta_n - \beta_m - l\frac{2\pi x}{\Lambda} = 0 \tag{7}$$

where β_m refers to the propagation constant of the m^{th} mode along the propagation direction, x; β_n refers to the propagation constant of the n^{th} mode along x, l indicates the order of the Fourier series term, and Λ is the period of the perturbation.

It should be noted that a stronger coupling coefficient between two modes leads to wider main lobes and higher side lobes. According to Eq. (6) if the modes in consideration are more tightly confined to the waveguides, the coupling coefficient will be weaker since there will be less overlap with the perturbation. This device was designed for the worst-case scenario, where the first CDC has a wider main lobe which leaves the possibility of light being coupled into the side lobes for the second CDC. To this end, WG_1 was chosen to be narrower than WG_3. The intermediate waveguide WG_2 was chosen to be the narrowest of the three. This maximizes the possible coupling coefficients for each CDC while maintaining same gap between each waveguide pair. This also allows for shorter device length for each CDC. The mode in WG_3 being more tightly confined that the mode in WG_1 leads to the overlap and hence the coupling coefficient being stronger for the WG_1-WG_2 pair, compared to that of WG_3-WG_2 pair. This leads to a wider main lobe for the grating in the WG_1-WG_2 pair. More detailed analysis and derivation about the coupled mode theory treatment can be found in [11,14].

The simulation data in Fig. 2 was obtained via 2.5D varFDTD simulations in LUMERICAL MODE. Each CDC had 600 periods which approximated to a device length of 0.19 mm per CDC. This was done to optimize the main lobe to side lobe contrast for each individual CDC. Beyond this point, the main lobe remained static, while the side lobes rose.

In this design the light couples from WG_1 to WG_2 via the first CDC (CDC_1). The main lobe for this CDC is wide. The light then encounters the second CDC (CDC_2) and gets coupled to WG_3. Here, the main lobe is narrower and the peak of the side lobe for CDC_2 overlaps with the minima of the main lobe for CDC_1. This leads to the reduction of the side lobe for CDC_2. It should be noted that it is essential to match the central wavelength for both CDCs. This ensures that the main lobes reinforce each other, and the strength of the main lobe remains unaffected for the light frequencies propagating in the cascade.

To ensure that the reduction of side lobes is being achieved by the overlap of minima of CDC_1 with the side lobe of CDC_2. Simulations were conducted where both WG_1 and WG_3 were the same. Consequently, both CDC_1 and CDC_2 have exactly same overlap. From Fig. 2(a) there is still some extra reduction with the side lobe after CDC_2 being 4.46 dB lower than the side lobe after CDC_1. But, for the device comprising of dissimilar CDCs, the side lobe is suppressed by 6.71 dB after CDC2 compared to the side lobe after CDC_1. As a result, the device with dissimilar CDCs has a side lobe reduction of 11.17 dB compared to 8.43 dB for similar CDCs. Hence, the effect of overlap between minima of main lobe and the maxima of the side lobe was verified.

Most importantly, the minimizing process of variation between the two CDCs was considered as a major impetus for the compact device design. Moreover, changes in the central wavelengths of the main lobe were observed while varying the minimum mesh size. This change becomes minimum after a certain number of mesh points. However, as we refine the mesh numerical error

Optics EXPRESS

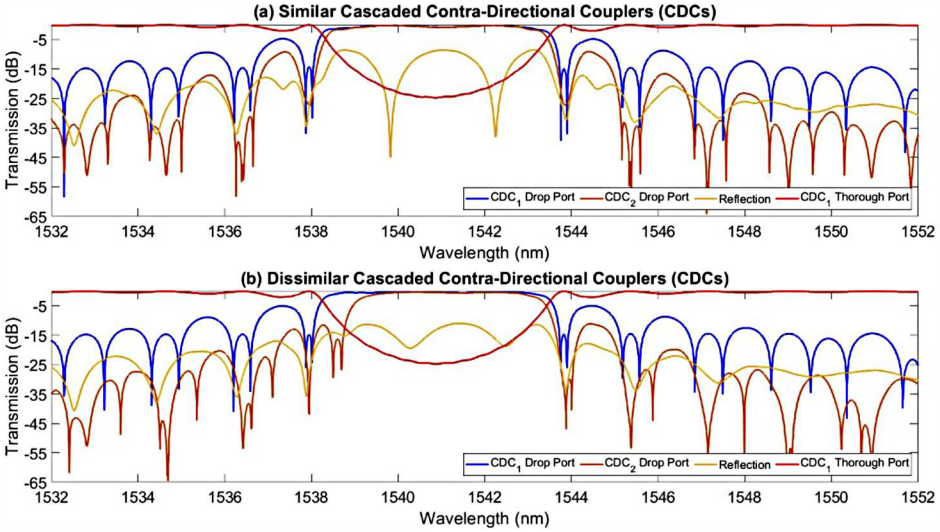

Fig. 2. LUMERICAL MODE - 2.5D varFDTD simulations of: (a) Similar cascaded contra-directional couplers (CDCs) in which the side mode reduction ratio of redirect segment of the incoming signal (through CDC_1) is approximately 3.97 dB and is lowered down to approximately 8.43 dB (through CDC_2). (b) Dissimilar cascaded contra-directional couplers (CDCs) in which the side mode reduction ratio of the redirect segment of the incoming signal (through CDC_1) is approximately 4.46 dB and is lowered down to approximately 11.17 dB (through CDC_2).

at each calculation point this also could lead to errors in simulations. From there, heaters were included even after performing the simulations at a very high level of mesh refinement.

3. Fabrication and characterization

The SOI device investigated in this manuscript was fabricated as part of a multi-project-wafer (MPW) run at the Applied Nano Tools foundry, Edmonton, Alberta, Canada [18]. In which a standard silicon on insulator (SOI) wafer with a 220-nm device layer is coated with a soft mask. The structures are then transferred into the device layer (fully etched) via electron beam lithography (EBL) and reactive ion etching (RIE). Plasma enhanced chemical vapor deposition (PECVD) is then employed to clad the sample with a thick layer (e.g., 2.2 μm) of silicon dioxide (SiO_2). Heaters are then formed by depositing Titanium-tungsten alloy (TiW) over the static Bragg gratings in order to tune the stop bands hence overcoming the overall fabrication variations. Titanium-tungsten aluminum bi-layers are then employed to route the heaters with contact pads. The device is then cladded with a thin layer (e.g., 300 nm) of silicon dioxide (SiO_2), which protects the heaters from oxidation. Small windows are opened on top of each pad via RIE [19]. The overall chip was designed to meet the design rules of Applied Nanotools where a complete listing of design rules and layout tools are reported in [18,20]. Moreover, detailed information regarding the fabrication process can be found in [18].

As illustrated in Fig. 1 and Fig. 3, The device consists of two static Bragg gratings (WG_1 and WG_3) and a mid-waveguide (WG_2) which is placed in between them. The width of the lower waveguide (WG_1) is chosen to be 500 nm where a portion of its sidewalls is periodically modulated by ± 25 nm and its grating period, Λ=320 nm with a 50% duty cycle (DC). The width of the upper waveguide (WG_3) is chosen to be 570 nm in which a portion of its sidewalls is periodically modulated by ± 25 nm and its grating period, Λ=315 nm with a 49.2% duty cycle

Optics EXPRESS

(DC). Both contra-directional couplers are formed out of 600 periods and are separated by a 200 nm gap from the 400 nm wide mid-waveguide (WG_2). The simulation results presented in Fig. 2(b) correspond to the final fabricated design.

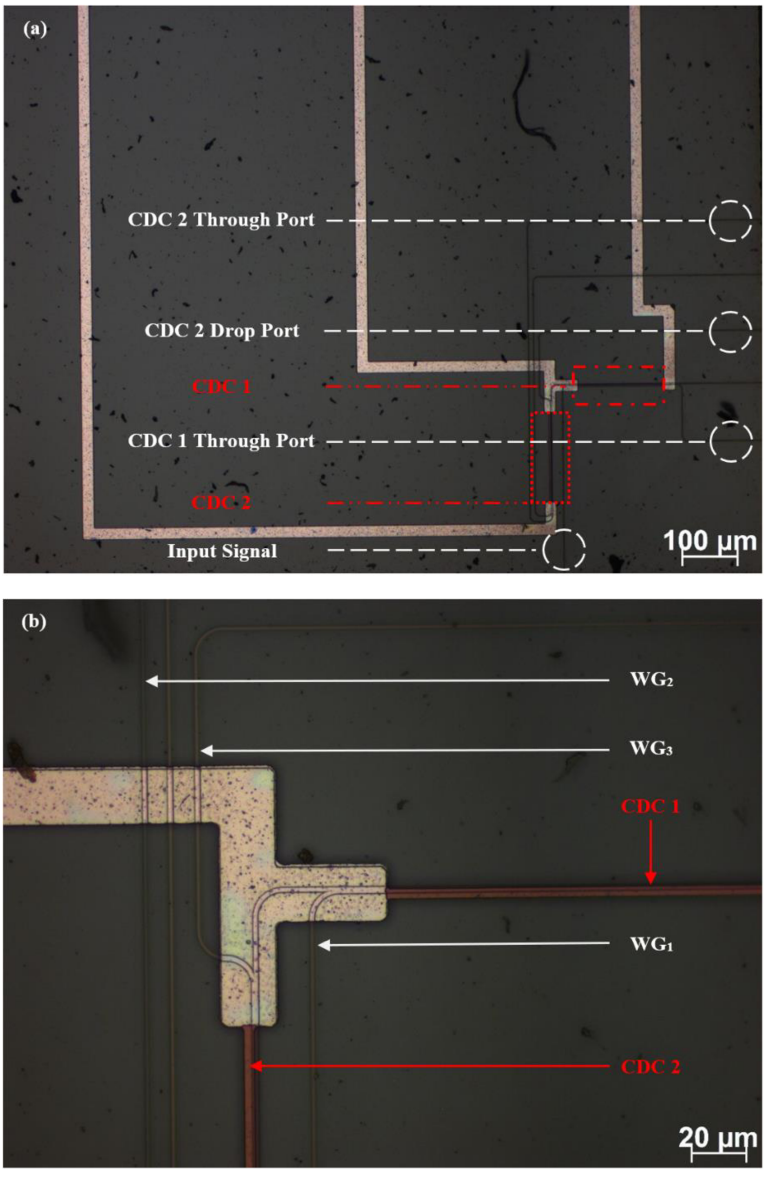

Fig. 3. Microscopic images of the chip showing: (a) The different input and output ports in addition to the two contra-directional couplers (image scale 100 µm). (b) The various waveguides (WG_1, WG_2, and WG_3) which create the two contra-directional couplers (image scale 20 µm).

The characterization of the side lobe reduction device was performed using a fiber-to-free space setup described in [21,22]. Moreover, the input/output waveguides on the chip were inversely tapered down to approximately 180 nm in an attempt to enhance the overall mode conversion

Optics EXPRESS

of the beam while coupling light from this setup. In addition, the CDCs were separated by approximately 40-45 um thus ensuring thermal isolation between them when tuning one of the individual heaters. This spacing was found to be sufficient according to LUMERICAL DEVICE Multiphysics Simulation (HEAT solver). Optimized heaters and trenches can then be employed in future devices that require even higher temperatures (tuning) or more compact designs.

4. Device performance

Without any adjustment to the heaters, the central wavelength for the CDCs main lobes were observed to be misaligned due to fabrication variation (as seen in Fig. 4(a)). In this case, CDC_2 Through port indicates the spectrum for CDC_1 Drop port. This was expected and was the primary impetus for the heaters being included in the design. Once 3.9 DC voltage (18.6 mA) was applied to the heater over CDC_1 the central wavelengths for both CDCs were aligned (see Fig. 4(b)). As it can be observed from Fig. 4(a), the side lobe for CDC_1 is approximately 5.57 dB below the main lobe. Once the CDCs are appropriately aligned, the side lobe for CDC_2 approximately overlaps with the null of the main lobe for CDC_1. As a result, the side lobe drops to 12.93 dB below the main lobe. This is a 7.36 dB improvement over the original performance of CDC_1.

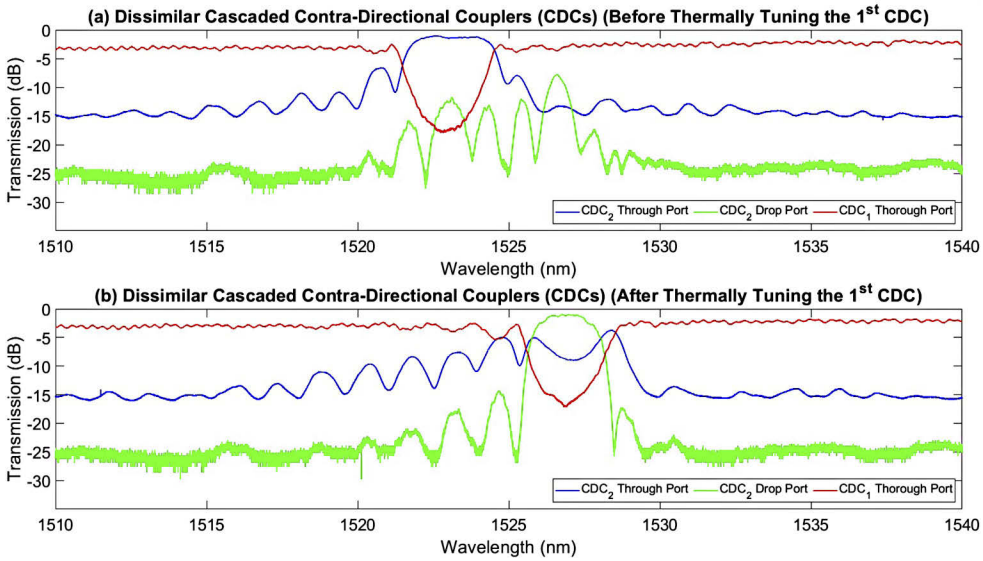

Fig. 4. Experimental characterization of the fabricated cascaded contra-directional couplers (CDCs): (a) Before thermally tuning the first CDC hence the central wavelength of the main lobe was misaligned in comparison to the second CDC (due to fabrication variation), therefore the side lobe of the second CDC does not overlap with the null of the main lobe (first CDC). In this case, CDC_2 Through port indicates the spectrum for CDC_1 Drop port. (b) After thermally tuning the first CDC hence the central wavelength of the main lobe aligns with that of the second CDC, therefore the side lobe of the second CDC overlaps with the null of the main lobe of CDC_1.

5. Discussion and conclusion

According to the simulations, the device shown here performs 2.74 dB better than a simple cascaded design. It should also be noted that for simple cascaded design, WG_1 and WG_3 will need to be placed a considerable distance apart to prevent any co-directional coupling. Another disadvantage for such design would be the potential for Fabry-Pérot resonances. Moreover, in

Optics EXPRESS

contrast to existing apodised designs with device lengths of around 1 mm, the novel dissimilar CDC cascade design has a much smaller footprint of 0.4 mm total length and a more controllable and predictable transmission spectrum. The compact nature of this design will allow for prevention of fabrication errors introduced in larger devices. In addition, the cascaded CDC design also doesn't broaden the main lobe of the device.

The design principal can be boiled down to reinforcement of main lobes by matching their centers while diminishing the side-lobes by overlapping the maxima of one coupler with the minima of the other. This basic principle can potentially be used to create devices with even better spectral characteristics if they require multiple CDCs or DBRs. One such widely popular use case would be the design of a DBR based laser cavity. When designing such a cavity, shorter DBR sections can be designed. Each DBR in this case will have worse main lobe to side lobe contrast compared to longer devices. However, if each of the DBRs is designed following the above design principle. The design could provide for a compact device with equal or better performance compared to a device with identical DBRs that have weaker coupling but are substantially longer. The design is highly adaptable and can also be used in case apodized DBR are required to meet performance specifications. Even when using apodized DBR, the individual DBR can be more compact leading to a smaller device footprint. It should also be noted that this device is expected to have slightly weaker reduction in one direction. In case of DBR lasers, such concerns will be minimized, since only the narrower main lobe that is being reinforced will survive multiple roundtrips in the cavity. The compact nature will allow for more reliable fabrication of these devices. This in turn will lead to better yields and lowering the cost per device and making the devices more market ready.

Funding. Defense Advanced Research Projects Agency (DSO NAC Programs); Office of Naval Research; National Science Foundation (ECCS-180789, NSF ECCS-190184, NSF ECCS-2023730); Army Research Office; San Diego Nanotechnology Infrastructure (SDNI) supported by the NSF National Nanotechnology Coordinated Infrastructure (ECCS-2025752); Quantum Materials for Energy Efficient Neuromorphic Computing-an Energy Frontier Research Center funded by the U.S. Department of Energy (DOE) Office of Science; Basic Energy Sciences (DE-SC0019273); LEED: A Lightwave Energy-Efficient Datacenter funded by the Advanced Research Projects Agency - Energy; Cymer Corporation.

Acknowledgments. Naif Alshamrani would like to thank King Abdulaziz City for Science and Technology (KACST) for their support during his study.

Disclosures. The authors declare no conflicts of interest.

Data availability. Data underlying the results presented in this paper are not publicly available at this time but may be obtained from the authors upon reasonable request.

References

1. W. Shi, X. Wang, C. Lin, H. Yun, Y. Liu, T. Baehr-Jones, M. Hochberg, N. A. F. Jaeger, and L. Chrostowski, "Silicon photonic grating-assisted, contra-directional couplers," Opt. Express **21**(3), 3633–3650 (2013).
2. J. A. Davis, A. Li, N. Alshamrani, and Y. Fainman, "Silicon photonic chip for 16-channel wavelength division (de-)multiplexing in the O-band," Opt. express **28**(16), 23620–23627 (2020).
3. C. K. Madsen and J. H. Zhao, *Optical Filter Design and Analysis: A Signal Processing Approach* (Wiley-Interscience, 1999).
4. D. Charron and W. Shi, "O-band add-drop filter in Bragg-grating-assisted Mach-Zehnder interferometers for CWDM," in *Conference on Lasers and Electro-Optics* (OSA, 2019), p. JTh2A.44.
5. Y. S. Fainman, J. Ford, W. M. Mellette, S. M. G. Porter, A. C. Snoeren, G. Papen, S. Saeedi, J. Cunningham, A. Krishnamoorthy, M. Gehl, C. T. DeRose, P. S. Davids, D. C. Trotter, A. L. Starbuck, C. M. Dallo, D. Hood, A. Pomerene, A. Lentine, S. Mookherjea, G. Porter, A. C. Snoeren, G. Papen, M. Gehl, C. T. DeRose, P. S. Davids, D. C. Trotter, A. L. Starbuck, C. M. Dallo, D. Hood, A. Pomerene, and A. Lentine, "LEED: A Lightwave Energy-Efficient Datacenter," in 2019 *Optical Fiber Communications Conference and Exhibition (OFC)* (OSA, 2019), pp. 1–3.
6. H. Qiu, J. Jiang, P. Yu, D. Mu, J. Yang, X. Jiang, H. Yu, R. Cheng, and L. Chrostowski, "Narrow-Band Add-Drop Filter Based on Phase-Modulated Grating-Assisted Contra-Directional Couplers," J. Lightwave Technol. **36**(17), 3760–3764 (2018).
7. X. Zhao, Y. Wang, Q. Huang, and J. Xia, "Two-mode contra-directional coupler based on superposed grating," Opt. Express **25**(3), 2654–2665 (2017).
8. J. St-Yves, H. Bahrami, P. Jean, S. LaRochelle, and W. Shi, "Widely bandwidth-tunable silicon filter with an unlimited free-spectral range," Opt. Lett. **40**(23), 5471–5474 (2015).

Optics EXPRESS

9. A. D. Simard, N. Belhadj, Y. Painchaud, and S. LaRochelle, "Apodized Silicon-on-Insulator Bragg Gratings," IEEE Photonics Technol. Lett. **24**(12), 1033–1035 (2012).
10. D. T. H. Tan, K. Ikeda, S. Zamek, A. Mizrahi, M. Nezhad, A. V. Krishnamoorthy, K. Raj, J. E. Cunningham, X. Zheng, I. Shubin, Y. Luo, and Y. Fainman, "Wide Bandwidth, Low Loss 1 by 4 Wavelength Division Multiplexer on Silicon for Optical Interconnects," in *Optical Fiber Communication Conference/National Fiber Optic Engineers Conference* 2011 (OSA, 2011), 19(3), p. OMM4.
11. H. Yun, M. Hammood, S. Lin, L. Chrostowski, and N. A. F. Jaeger, "Broadband flat-top SOI add–drop filters using apodized sub-wavelength grating contradirectional couplers," Opt. Lett. **44**(20), 4929–4932 (2019).
12. P. S. Cross and H. Kogelnik, "Sidelobe suppression in corrugated-waveguide filters," Opt. Lett. **1**(1), 43–45 (1977).
13. A. Karimi, F. Emami, and N. Nozhat, "The effects of various apodization functions on the filtering characteristics of the grating-assisted SOI strip waveguides," J. Opt. Soc. Korea **18**(2), 101–109 (2014).
14. S. Kumar, "Design and Manipulation of On-Chip Bragg Couplers for Side Lobe Suppression," University of California, San Diego (2018).
15. A. Yariv and P. Yeh, *Optical Waves in Crystals: Propagation and Control of Laser Radiation* (Wiley-Interscience, 2003).
16. J.-P. Weber, "Spectral characteristics of coupled-waveguide Bragg-reflection tunable optical filter," IEE Proc.-J: Optoelectron. **140**(5), 275–284 (1993).
17. K. Ikeda, M. Nezhad, and Y. Fainman, "Wavelength selective coupler with vertical gratings on silicon chip," Appl. Phys. Lett. **92**(20), 201111 (2008).
18. "NanoSOI Fabrication Process | Applied Nanotools Inc.," https://www.appliednt.com/nanosoi/.
19. N. Alshamrani, A. Grieco, A. Friedman, K. Johnson, M. S. Kim, F. Floris, P. O'brien, and S. Fainman, "A Non-Mechanical Multi-Wavelength Integrated Photonic Beam Steering System," J. Lightwave Technol. **39**(12), 4201–4208 (2021).
20. L. Chrostowski, Z. Lu, J. Flueckiger, X. Wang, J. Klein, A. Liu, J. Jhoja, and J. Pond, "Design and simulation of silicon photonic schematics and layouts," in *Proc.SPIE*, L. Vivien, L. Pavesi, and S. Pelli, eds. (2016), 9891, p. 989114.
21. N. Alshamrani, A. Grieco, B. Hong, and Y. Fainman, "Miniaturized integrated spectrometer using a silicon ring-grating design," Opt. Express **29**(10), 15279–15287 (2021).
22. A. Grieco, B. Slutsky, D. T. H. Tan, S. Zamek, M. P. Nezhad, and Y. Fainman, "Optical bistability in a silicon waveguide distributed bragg reflector Fabry-pérot resonator," J. Lightwave Technol. **30**(14), 2352–2355 (2012).